Modeling NO_2 concentrations in real urban areas using computational fluid dynamics: A comparative analysis of methods to assess NO_2 concentrations from NO_x dispersion results

Nicolas Reiminger[1,2,†,*], Xavier Jurado[1,*], Loïc Maurer[3], José Vazquez[3], Cédric Wemmert[2]

[1]*AIR&D, 32 rue Wimpheling, F-67000, Strasbourg, France*
[2]*ICube Laboratory, UMR 7357, CNRS/University of Strasbourg, F-67000, Strasbourg, France*
[3]*Université de Strasbourg, CNRS, ENGEES, ICube UMR 7357, Département Mécanique, F-67000, Strasbourg, France*

* These authors contributed equally to this work
† Corresponding author: Tel. +33 (0)6 31 26 75 88, Mail. nreiminger@air-d.fr

---

Citation : Reiminger, N., Jurado, X., Maurer, L., Vazquez, J., & Wemmert, C. (2024). Modeling NO2 concentrations in real urban areas using computational fluid dynamics: A comparative analysis of methods to assess NO2 concentrations from NOx dispersion results. Sustainable Cities and Society, 103, 105286.
https://doi.org/10.1016/j.scs.2024.105286

Abstract: Major cities worldwide constantly deal with health hazards caused by air pollution. Modeling this pollution on an urban scale is essential for assessing the impact of local policies and promoting sustainable urban development. However, there are practical difficulties when using microscale modeling in applied context, and particularly for nitrogen dioxide modeling (NO_2). In this study, a Computational Fluid Dynamics (CFD) model was employed to assess monthly NO_2 concentrations in Antwerp, Belgium, and the results were compared to a one-month measurement campaign using 73 passive samplers. The result showed that using CFD with conventional assumption – such as neutral atmospheric stability consideration and using a turbulent Schmidt number (Sc_t) set to 0.7 – yield satisfying results according to air quality model acceptance criteria. Optimal outcomes were achieved by considering NO_2 background concentration instead of NO_x and employing Bachlin et al.'s empirical function to convert modeled NO_x concentrations to NO_2, dismissing the need for straightforward chemical mechanisms – such as photostationary steady-state equilibrium (PSS) –, or more expensive models in terms of computing resources. This approach yielded an overall error of less than 15 % and a correlation coefficient R of 0.78, affirming its effectiveness in modeling NO_2 air quality in applied context.

Keywords: Computational fluid dynamics, Air quality, Microscale modeling, Nitrogen dioxide, NO2

Highlights:

- NO_2 concentrations can be effectively modeled without any chemical mechanism
- Less than 15% of error is obtained using the Bachlin et al. empirical function
- Neutral atmosphere and Sct = 0.7 yields good results in real application

1. Introduction

Air pollution is one of the major concerns of the last few decades, leading to a decline in well-being, quality of life and life expectancy by several years (Manisalidis et al., 2020). Consequently, it has become a prominent challenge for modern societies (Agathokleous and Sicard, 2021).

Among the various pollutants found in the atmosphere, nitrogen dioxide (NO_2) has been identified by the World Health Organization (WHO) as one of the highest priority air pollutants to be monitored (WHO, 2005). This pollutant is multifaceted in its detrimental effects. On the human health front, it has been linked to various disorders such as lung diseases (Yue et al., 2022), asthmatic symptoms (van Zoest et al., 2020), and chronic kidney diseases (Wu et al., 2022), among others. Environmentally, it acts as a precursor to nitric acid production in the atmosphere, playing a significant role in the formation of acid rain (Sudalma et al., 2015). This not only underscores its direct impact on human health but also highlights its broader ecological consequences. Furthermore, this airborne pollutant is also one of the most frequently encountered air pollutants in urban areas. Its primary sources are anthropogenic, predominantly stemming from industrial activities and, to a greater extent, traffic exhaust emissions (Thunis, 2018). For instance, in Paris, France, more than half (56 %) of the total NO_x emissions (including primary-emitted and secondary-formed NO_2) come from traffic-related emissions, while less than 20 % comes from tertiary and residential sectors (AIRPARIF, 2016). In the meantime, there exists a paradox: living in urban areas, particularly near high-traffic roads, is associated with elevated health risks (Chen et al., 2017; Finkelstein et al., 2004). Despite this, there is a growing trend of urbanization, with the global urban population projected to increase from the current 50% to 68% by 2050 (United Nations, 2019).

To protect populations from excessive exposure to air pollution, the European Union (EU) and the WHO have issued critical values of NO_2 concentrations not to be exceeded which include hourly and annual standards (EU, 2008; WHO, 2021). To use these standards, it is therefore essential to have the capability to accurately assess NO_2 concentrations, which is a matter of its own.

There are two distinct methods to assess NO_2 concentrations in ambient air: measurement campaigns and numerical modeling. Although the first approach provides real information from the field, it suffers from some limitations such as spatial representativeness, both horizontally and vertically, as well as the time and cost involved in collecting sufficient data associated with the corresponding costs (Jurado et al., 2023a). Numerical modeling, on the other hand, can surmount these limitations, facilitating the development of new strategies to enhance air quality in urban areas. This is achievable through the consideration of both emission patterns and urban morphology scenarios (Yang et al., 2020), assuming the models are optimally utilized.

Among the existing numerical modeling approaches, Computational Fluid Dynamics (CFD) has shown a strong interest over the past decades for computational wind engineering (Blocken, 2014) and, more specifically, for air quality modeling purposes in urban areas (Pantusheva et al., 2022). Indeed, such numerical model has been widely used to assess the impact of street canyon layouts (Xiaomin et al., 2006), building shapes (Li et al., 2020), roof shapes (Kluková et al., 2021), road morphologies (Reiminger et al., 2023) or vegetation effects (Santiago et al., 2017) on the air quality. CFD, nonetheless, suffers from some practical issues when used to assess air quality in real urban areas for engineering purposes. A first questioning factor is about the turbulent Schmidt number (Sc_t) which is a key parameter in CFD modeling of air pollution. However, this number is depending on a variety of parameters (e.g., numerical model, turbulence model, building layout, etc.). Previous studies show that the turbulent Schmidt number can vary between 0.2 and 1.3, mostly depending on the dominant effect in the turbulent mass transport (Tominaga and Stathopoulos, 2007),

raising the question of the value to be considered for applied studies. A second issue that can be mentioned is the assumption of isothermal conditions (neutral atmospheric stratification), facilitating both calculation and results processing, but ignoring the impact of atmospheric stability and associated thermal phenomena. This assumption is widely accepted (Pantusheva et al., 2022), except in specific study cases where significant differences in pollutant concentrations were observed compared to the neutral (nonthermal) case results, both leading to the underestimation and overestimation of pollutant concentrations (Reiminger et al., 2020a).

Lastly, there is also a major issue specifically related to NO_2 modeling. While NO_x can be considered as a non-reactive pollutant and directly modeled through CFD (Sanchez et al., 2016), NO_2 is highly reactive, especially with ozone (O_3), and its concentrations depend on complex chemical mechanisms as well as on the concentrations of many other chemical species. According to Sanchez et al. (2017), these mechanisms which also involve air temperature and solar radiation should be accounted for in CFD modeling to avoid errors in NO_2 concentration predictions, while Jurado et al. (2023b) show more recently that simple empirical equations are sufficient to predict NO_2 concentrations from NO_x modeled maps.

Based on these observations, the objective of this study is twofold. Primarily, it aims to evaluate the accuracy of straightforward and rapid methods for estimating NO_2 concentrations from NO_x CFD dispersion results, bypassing the need for intricate explicit chemical mechanisms. Then, it is also to ensure that common CFD modeling assumptions, including using 0.7 as the turbulent Schmidt number and only considering neutral atmosphere conditions without any thermal effect, are relevant for air quality modeling in urban areas, i.e., with the goal of obtaining reliable results.

To achieve these objectives, several CFD simulations were performed in the city of Antwerp, Belgium, and the results of different methodologies for calculating NO_2 concentrations from NO_x concentrations were compared with on-site monitoring data. All details about the study location, data availability, numerical model used, methodologies assessed, and performance criteria considered are given in Section 2. Then, the results of the study are exposed in Section 3 and discussed in Section 4. Finally, the conclusions of this work are drawn in section 5.

2. Material and methods

2.1. Study location and data availability

The study was carried out in Antwerp, Belgium. This city is characterized by a flat topography and a typical urban layout of large Western European cities, with densely built-up areas, street canyons and open areas. The Flemish Environment Agency (VMM) conducted numerous measurement campaigns and investigations in Antwerp throughout 2016. These data include monitored NO_2 concentrations, modeled background concentrations, calculated traffic emissions and observed building layouts and weather data. These data, owned by VMM, have been made available to the FAIRMODE (Forum for Air quality Modeling) scientific community. They were utilized in this study for the purpose of comparing them against numerical results.

2.1.1. NO_2 air quality measurement campaigns

A monthly measurement campaign has been carried out by the VMM from April 30th to May 28th, 2016. In this campaign, NO_2 concentrations were monitored at 73 locations of various heights (from 2.7 m to 10.8 m) using passive samplers.
Measurement of NO_2 concentration using passive samplers is based on the principle of diffusion of nitrogen dioxide onto an absorbent support during the measurement

campaign, which is then analyzed in the laboratory, leading to an average concentration over the campaign period.

Collection, validation, and quality control of the sampling have been carried out following the procedure described in De Craemer et al. (2020), in line with demands and expectations of the European union in terms of quality of results for measurement campaigns (maximum deviation of 30 %). Still according to these authors, the actual maximum deviation of the passive samplers is less than 10 %.

Available data correspond to monthly NO_2 concentrations at these 73 locations. Figure 1 displays a satellite image of Antwerp, indicating the location of the passive samplers by distinguishing passive samplers located near roads where information on traffic, and therefore emissions, is available (depicted in yellow), from those where this information is not available (depicted in white). This distinction is used later in the results section.

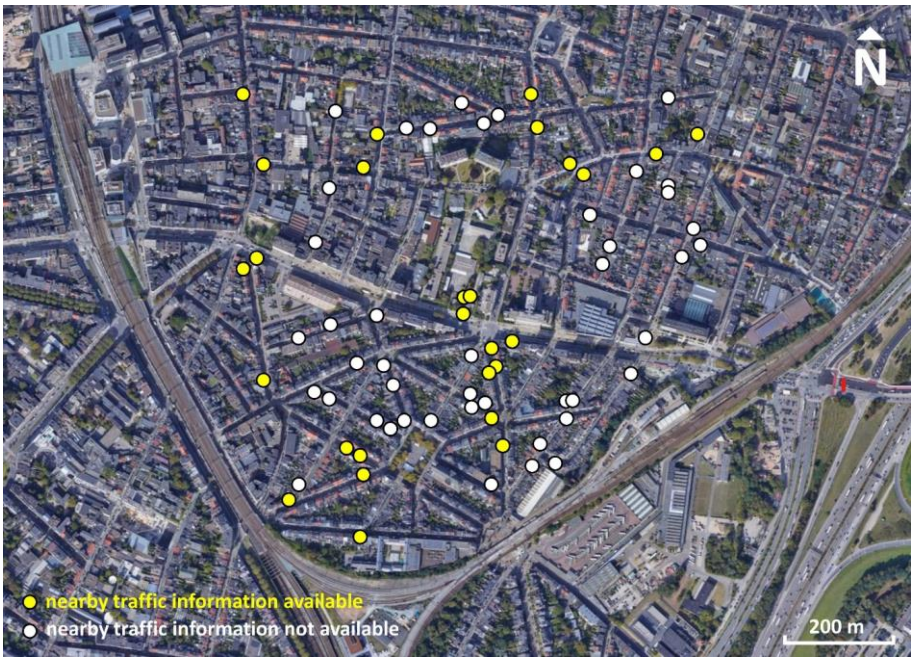

Figure 1. Satellite map showing the location of passive samplers used in this study. Samplers near roads with known traffic information are marked in yellow, while those in areas lacking traffic information from the data provider are marked in white.

2.1.2. Background concentration

The background concentrations correspond to results obtained by the VITO (Flemish Institute for Technological Research), using the RIO model (Janssen et al., 2008). This model used land use regression and measurement data to assess hourly NO_2 and NO_x background air pollution concentrations. The monthly background concentrations over the measurement campaign period are $\overline{NO_{2\ bg}} = 27.6$ µg/m³ and $\overline{NO_{x\ bg}} = 34{,}3$ µg/m³.

2.1.3. Emission data

There are no major industrial sources of air pollution in the study area. The pollution observed is therefore mainly influenced by emissions from road traffic and its dispersion and accumulation as a function of Antwerp's urban characteristics (street canyons, open areas, etc.). More distant sources of pollutants are, for their part, included in the background concentrations (see Section 2.1.2.).

Traffic emission data were obtained using the Fastrace Traffic Model (version 2.1), considering the official traffic and fleet data of 2016 from the Department for Mobility and based on the COPERT 5 emission factors.

2.1.4. Buildings data

The buildings data corresponds of 3D polygons (2D sketch with associated heights) acquired from the 3D GRB Informatic Vlaanderen (LOD I)[1]. Most of the buildings are two to three storeys high and are mainly commercial and residential. Large public gardens and smaller private gardens are also scattered throughout the area.

2.1.5. Weather data

Weather data were monitored at the Antwerp-Luchtbal measurement station, located 5 km north of the studied area (coordinates: 51.261, 4.425). These data include hourly measurements of averaged wind direction, wind speed, relative humidity, temperature, and total radiation and cover the entire year of 2016.
The resulting wind rose during the measurement campaign as well as the atmospheric stability statistics are given in Figure 2.

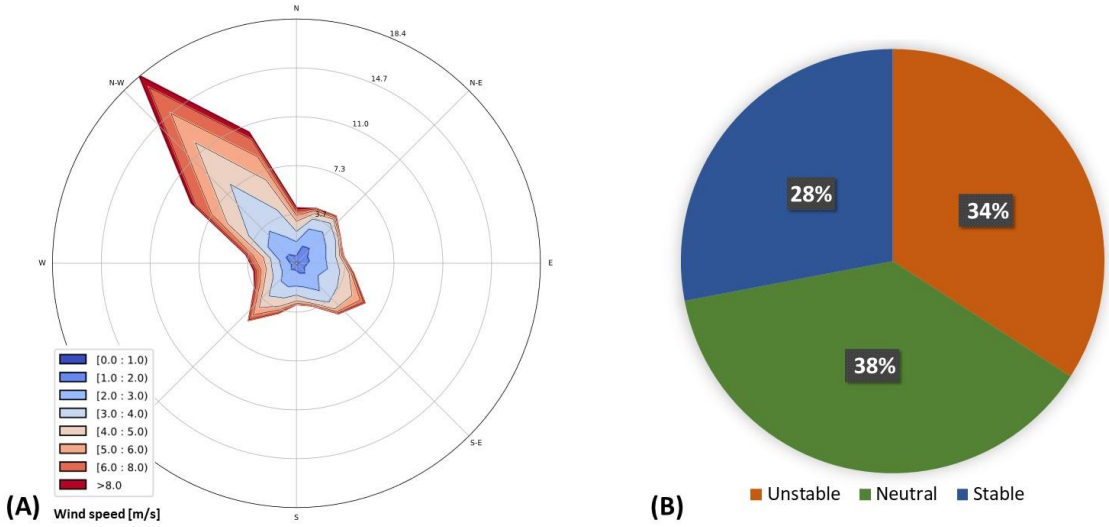

Figure 2. Meteorological data including (A) the wind rose giving wind speed and direction statistics in Antwerp between April 30th and May 28th, 2016 (N, North, signify that wind is coming from the North and going to the South) and (B) atmospheric stability statistics.

2.2. Numerical model

2.2.1. Software and calculation methodology

Simulations were performed through OpenFOAM 9, working in parallel calculation on a 32-core Intel® Xeon(R) Silver 4216 CPU E5-2670 2.10 GHz computing machine under Ubuntu 20.04.5 LTS.

The CFD solver used is *pimpleFoam*, a transient forced convection solver from the OpenFOAM library. This solver is capable of solving the incompressible Navier-Stokes equations for isothermal flows, thereby limiting the modeling to neutral atmospheric

[1] Data available here: https://overheid.vlaanderen.be/grb-3dgrb

stability. However, according to Figure 2 (B), this condition is only accurate 38% of the time, which is an additional point of investigation in this work. The solver has been modified to account for passive pollutant dispersion since it does not natively allow it.

The URANS (Unsteady Reynolds-Averaged Navier-Stokes) methodology has been used to solve the equations, as substantially better results can be achieved using transient calculation rather than steady calculation (Tominaga and Stathopoulos, 2017). Employing a RANS methodology introduces the Reynolds Stress Tensor term in the Navier-Stokes momentum equation, then requiring the choice of a turbulent closure scheme. The Renormalization Group (RNG) k-ε model from Yakhot et al. (1992) has been selected to solve this new term, since better results can be achieved using it (Papageorgakis and Assanis, 1999) while much more complex closure schemes may not improve the results but increase calculation costs (Koutsourakis et al., 2012).

The modified *pimpleFoam* solver, the use of the URANS methodology and the RNG k-ε turbulence closure scheme for pollutant dispersion purpose were validated in a previous study on both velocity and pollutant concentration fields based on experimental data (Reiminger et al., 2020c).

2.2.2. Governing equations

The incompressible Navier-Stokes equations solved by the *pimpleFoam* solver are given as follows, with (1) the continuity equation and (2) the momentum equation:

$$\nabla . u = 0 \qquad (1)$$

$$\frac{\partial u}{\partial t} + u . \nabla u = -\frac{1}{\rho}\nabla p + \nu \Delta u \qquad (2)$$

where u is the velocity [m.s^{-1}], t the time [s], ρ the density [kg.m^{-3}], p the pressure [Pa or kg.m^{-1}.s^{-2}] and ν the kinematic viscosity [m^2.s^{-1}]

The advection-diffusion equation, governing passive scalar transport, was used to model pollutant dispersion since no explicit chemical reactions were considered in this study. The corresponding equation is given in equation (3), as follows:

$$\frac{\partial C}{\partial t} + \nabla . (Cu) - \nabla . \left[\left(D_m + \frac{\nu_t}{Sc_t} \right) \nabla C \right] = E \qquad (3)$$

where C is the pollutant concentration [g.m^{-3}], t is the time [s], u is the velocity [m.s^{-1}], D_m is the molecular diffusion coefficient [m^{-2}.s^{-1}], ν_t is the turbulent diffusivity [m^{-2}.s^{-1}], Sc_t is the turbulent Schmidt number [-] and E is the emission of pollutants [g.s^{-1}].

While the turbulent Schmidt number can vary between 0.2 and 1.3 depending on the case to be modeled (Tominaga and Stathopoulos, 2007), an intermediate value of 0.7 frequently found in the literature (Rivas et al., 2019; Tominaga and Stathopoulos, 2017; Yuan et al., 2017) was used, which is an additional point of investigation in this work.

2.2.3. Computational domain and boundary conditions

Simulations were performed considering fully three-dimensional geometries, following traffic and building layout data available in Antwerp (see Section 2.1.3 and 2.1.4). An overview of the 3D numerical model is given in Figure 3, with, in red, the roads where emission data were available and modeled.

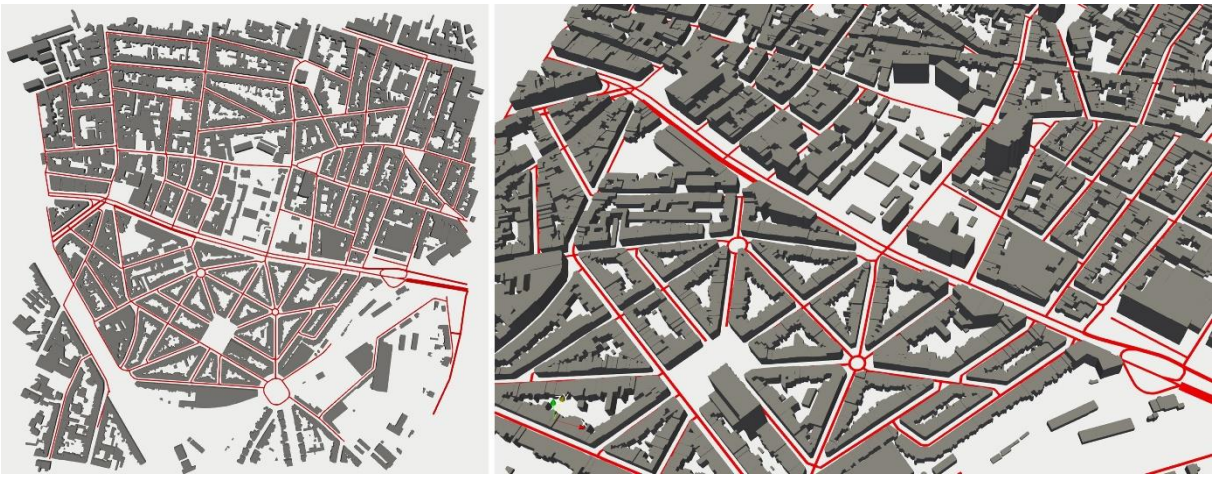

Figure 3. Overview of the 3D numerical model with (A) a top view and (B) a three-quarter view (red lines correspond to roads for which emission data were available and were modeled).

Mesh size of 1 m near wall boundaries (buildings and ground) were used as in Sanchez et al., (2017) or Vranckx et al. (2015), with, nevertheless, a higher refinement of 0.5 m close to pollutant sources (roads). This mesh resolution yielded numerical models comprising around 17 million meshes.
All the recommendations concerning domain size and boundary conditions given in COST Action 732 (Franke et al., 2007) were followed for each simulation performed, including:

- Inlet boundaries located $5H_{max}$ away from the first building, where velocity (4) and turbulence (5-6) profiles specified according to Richards and Hoxey (1993) and Richards and Norris (2011);
- Outlet boundaries located $5H_{max}$ away from the last building, where a free stream condition is applied to allow a fully development of the flow;
- Lateral boundaries located $5H_{max}$ away from the last building, where symmetry conditions are applied;
- Top boundaries located $5H_{max}$ away from the higher building ($5H_{max}$ from the ground), where a symmetry condition is applied.
- Ground and building wall boundaries where no-slip conditions (U = 0 m.s^{-1}) are applied.

$$U = \frac{u_*}{\kappa} ln\left(\frac{z + z_0}{z_0}\right) \qquad (4)$$

$$k = \frac{{u_*}^2}{\sqrt{C_\mu}} \qquad (5)$$

$$\varepsilon = \frac{{u_*}^3}{\kappa . z} \qquad (6)$$

where U is the wind velocity [m.s^{-1}], k is the turbulent kinetic energy [m^2.s^{-2}], ε is the turbulence dissipation rate [m^2.s^{-3}], u_* is the friction velocity [m.s^{-1}], κ is the von Kármán constant [-] taken to 0.41, z is the altitude [m], z_0 is the roughness height [m] taken as 0.5 m to stand for built-up areas (Hahmann et al., 2015; Troen and Petersen, 1989) and C_μ is a CFD constant [-] taken as 0.085.

Traffic exhaust emissions were modeled using volumetric pollutant sources along the roads and over one mesh height (0.5 m), considering emissions of each road segment.

Simulations were performed using second order schemes for all divergent, gradients and Laplacians terms and were run until full convergence, leading to residuals under 10^{-5}.

Lastly, it should be noted that the simulations were conducted under isothermal conditions (neutral atmosphere) and without traffic-induced turbulence. Consequently, pollutant concentrations are solely dependent on wind direction (Schatzmann and Leitl, 2011). Thus, a total of 18 wind directions were modeled using a 20° step (0°N, 20°, …, 320°N and 340°N) considering a wind speed of 1.5 m.s^{-1} at 10 m height. Concentrations from non-simulated wind speeds ($U_{H=10m} \neq$ 1.5 m.s^{-1}) were then obtained following equation (7) (Reiminger et al., 2020b).

$$C_u = U_{ref}.\frac{C_{ref}}{u} \qquad (7)$$

where C_u is the pollutant concentration for the wind velocity u not simulated and C_{ref} the reference pollutant concentration for the simulated wind velocity U_{ref}.

2.3. Methodologies to compute NO_2 from NO_x

2.3.1. NO_2/NO_x models

Considering the hourly wind speed and wind direction data available from April 30th to May 28th, 2016, a total of 696 hourly NO_x concentration maps were obtained from the 18 CFD simulations. Then, several methods were considered and compared to assess NO_2 concentrations from the NO_x maps results. These methods will hereafter be referred to as "NO_2/NO_x models".
The NO_2/NO_x models considered in this work include:

- A simplified chemical mechanism following the Leighton's relationship (Leighton, 1961) given in equation (8). This mechanism, called the Photostationary Steady States (PSS) equilibrium, can be solved following equations (9-11), and will be referred as *PSS model* in the results section.

$$[O_3] = \frac{J_{NO_2}[NO_2]}{k_{O_3}[NO]} \qquad (8)$$

$$[NO_2]_{PSS} = [NO_x]\frac{k_{O_3}[O_3]}{J_{NO_2}}\left(1 + \frac{k_{O_3}[O_3]}{J_{NO_2}}\right)^{-1} \qquad (9)$$

$$J_{NO_2} = 0.0167.e^{-0.575.\sec(\theta)} \qquad (10)$$

$$k_{O_3} = \frac{15.33}{T}.e^{-1450/T} \qquad (11)$$

  where $[NO_2]$, $[NO]$, $[NO_x]$ and $[O_3]$ are nitrogen dioxide, nitrogen monoxide, nitrogen oxides and ozone concentrations [g.m^{-3}], respectively, J_{NO_2} the photolysis frequency [s^{-1}] from Dickerson et al. (1982) with θ the solar zenithal angle [-] and k_{O_3} the reaction rate between NO, O_3, NO_2 and O_2 [ppb^{-1}.s^{-1}] from (Hanrahan, 1999) with T the temperature [K].

- The polynomial-logarithmic empirical function from Derwent and Middleton (1996) linking NO_2 concentrations to NO_x concentrations, given in equations (12-13), which is referred to as *DE model* in the result section.

$$[NO_2] = \left(2.166 - \frac{[NO_x]}{1.91}(1.236 - 3.348\,A + 1.933\,A^2 - 0.326\,A^3)\right) \times 1.91 \qquad (12)$$

$$A = log_{10}([NO_x]/1.91) \qquad (13)$$

where $[NO_2]$ and $[NO_x]$ are nitrogen dioxide and nitrogen oxides concentrations [g/m^3], respectively.

- The rational empirical function from Bächlin et al. (2008) linking NO_2 concentrations to NO_x concentrations, given in equations (14) , which is referred to as *BA model* in the result section.

$$[NO_2] = \frac{29.[NO_x]}{[NO_x]_a + 35} + 0.217\,[NO_x] \qquad (14)$$

where $[NO_2]$ and $[NO_x]$ are nitrogen dioxide and nitrogen oxides concentrations [g/m^3], respectively.

It should be noted that the empirical functions given in equations (12), (13) and (14) were previously mentioned and studied by Jurado et al. (2020) to assess NO_2 concentrations from monitored NO_x concentrations and lead to an overall deviation of 10% over the whole of France.

2.3.2. Calculation decomposition

The NO_2/NO_x models can then be applied at various stages of the calculation process to generate the maps of averaged NO_2 concentrations, which are influenced by:

- When the hourly results are averaged to obtain the monthly concentrations: before (17-18) or after (15-16) calculating NO_2 from NO_x with the NO_2/NO_x models.
- How the background concentration is included: before NO_2 calculation using NO_x background concentration (15, 17), or after, using NO_2 background concentration (16, 18).
-

The four equations combining these two possibilities are given hereafter in equations (15-18) and were all considered in this work for comparison purpose. These different ways of breaking down NO_2 calculations will be referred to as "calculation decomposition".

$$\overline{[NO_2]} = \frac{1}{n}\sum_{h=1}^{n} f([NO_x]_h + [NO_x]_{bg,h}) \qquad (15)$$

$$\overline{[NO_2]} = \frac{1}{n}\sum_{h=1}^{n} f([NO_x]_h) + \frac{1}{n}\sum_{h=1}^{n} [NO_2]_{bg,h} \qquad (16)$$

$$\overline{[NO_2]} = f\left(\frac{1}{n}\sum_{h=1}^{n} [NO_x]_h + [NO_x]_{bg,h}\right) \qquad (17)$$

$$\overline{[NO_2]} = f\left(\frac{1}{n}\sum_{h=1}^{n} [NO_x]_h\right) + \frac{1}{n}\sum_{h=1}^{n} [NO_2]_{bg,h} \qquad (18)$$

where f is one of the three NO_2/NO_x models described in Section 2.3.1, $\overline{[NO_2]}$ is the monthly NO_2 concentration, $[NO_x]_h$ is the hourly modeled NO_x concentration, $[NO_x]_{bg,h}$ is the hourly NO_x background concentration and $[NO_2]_{bg,h}$ is the hourly NO_2 background concentration. All these concentrations are in µg/m^3.

In the results section, the decompositions methods given in equation (15) is referred to as *H. NO_x*, equation (16) to *H. NO_2*, equation (17) to *Avg. NO_x* and equation (18) to *Avg. NO_2*.

2.4. Performance criteria

Several performance criteria were employed to evaluate and compare the effectiveness of the NO_2/NO_x models and calculation decompositions against the data from the measurement campaign, including: $\boldsymbol{FAC2}$ (factor of modeled values within a factor of two of observations), $\boldsymbol{FB}$ (Fractional Bias), $\boldsymbol{MFB}$ (Mean Fractional Bias), $\boldsymbol{MFE}$ (Mean Fractional Error), $\boldsymbol{NMSE}$ (Normalized Mean Squared Error), $\boldsymbol{MRE}$ (Mean Relative Error), $\boldsymbol{R}$ (Pearson correlation coefficient), $\boldsymbol{NSD}$ (Normalized Standard Deviation) and $\boldsymbol{Target}$. The corresponding equations are detailed in Appendix A, and all the results for these parameters are given to make it easier to compare the results of this work with others.

3. Results

3.1. Quantitative comparison of the NO_2/NO_x models and calculation decomposition results considering the whole dataset

Predicted NO_2 concentrations were initially compared to the complete set of measured NO_2 concentrations using observation versus prediction graphs. The corresponding graphs are presented in Figure 4 for each NO_2/NO_x model and calculation decomposition method considered in this study. Additionally, their corresponding correlation coefficients R and mean relative errors $MREs$ were calculated and given in the figure.

Firstly, by comparing the use of the NO_2 or NO_x background concentrations, it can be observed that predictions are systematically closer to the observed NO_2 concentrations when the background NO_2 concentration is considered rather than that of NO_x. Indeed, considering the NO_x background concentration led to $MREs$ ranging from 38 % to 63 %, while these errors are two to three times lower (between 16 % and 19 %) when considering the NO_2 background concentration instead. The correlation coefficients in both cases are similar, ranging from 0.73 to 0.75.

Secondly, comparing the use of hourly or averaged NO_x modeled concentrations in the decomposition model, the results are globally better using the averaged values rather than using the hourly ones. For example, considering the Derwent and Middleton NO_x/NO_2 model with the NO_x background concentration led to 38 % of mean relative error with averaged concentration, while 50 % of error is obtained with the hourly concentrations. This observation holds when considering the NO_2 background concentration. However, it is somewhat less pronounced in the case of the Bachlin et al. model, while there is no discernible difference for the Derwent and Middleton model. Finally, if we compare the results of the NO_2/NO_x models one by one considering the same calculation decomposition method, it appears that all the models lead to results with errors of the same order of magnitude. The best predictions based on R, $MREs$ and predicted versus observed plots are obtained considering the Bachlin et al. NO_2/NO_x model (eq. 14), and the calculation decomposition method which uses averaged predicted concentration values and NO_2 background concentration (eq. 18).

Additional performance criteria have been calculated to go further in the investigation of the best models and methods to be used. These criteria as well as R and $MREs$ already discussed are given in Table 1. According to the results, some criteria do not necessarily provide sufficient information to rank the different models or methods. Indeed, as previously, it is the case for the correlation coefficient (R), but it is also true for the factor of modeled values within a factor of two of observations ($FAC2$) which are ranging from 0.97 to 1.00. Then, other criteria such as FB, MFB, MFE, $NMSE$ and MRE tend to give around the same results when considering a given calculation decomposition method, whatever the NO_2NO_x model considered. They can therefore be used to rank the calculation decomposition methods, but not the NO_x/NO_2 models. The last criteria, including NSD and $Target$, give different results whatever the model or

method considered. They therefore appear to be the most stringent criteria. According to the $Target$, the photo stationary steady-state equilibrium (PSS) appears to be the best NO_2/NO_x model when using hourly predicted concentrations, while the Derwent and Middleton model is the best when using averaged concentrations. Based on the $Target$ criterion, the second option appears to be the more favorable of the two.

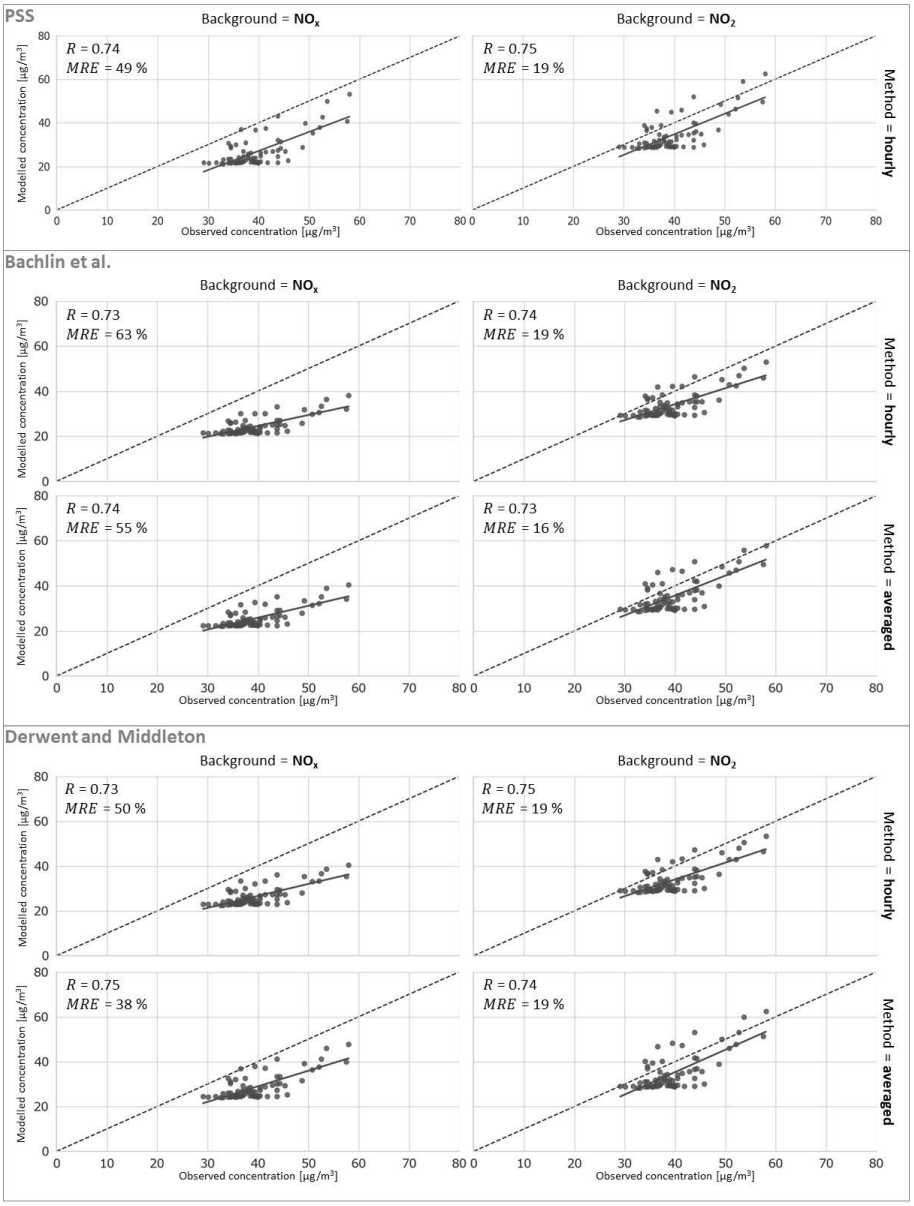

Figure 4. Comparison between observed and modeled NO_2 concentrations as a function of the NO_x/NO_2 model (PSS, Bachlin et al. or Derwent and Middleton models) and the calculation decomposition (hourly decomposition with NO_x or NO_2 background concentration or averaged decomposition with NO_x or NO_2 background concentration) considered.

Table 1. Comparison of the NO_x/NO_x models performances as a function of the calculation decomposition used.

Calculation decomposition	NO_x/NO_2 model	*FAC2*	*FB*	*MFB*	*MFE*	*NMSE*	*MRE*	*R*	*NSD*	*Target*
Hourly, NO_x background, eq. (15)	PSS	0.97	0.40	0.54	0.54	0.19	0.49	0.74	0.84	1.96
	Derwent and Middleton	1.00	0.40	0.51	0.51	0.18	0.50	0.73	1.37	3.16
	Bächlin et al.	0.97	0.48	0.64	0.64	0.26	0.63	0.73	1.53	3.97
Hourly, NO_2 background, eq. (16)	PSS	1.00	0.14	0.18	0.20	0.04	0.19	0.75	0.78	0.96
	Derwent and Middleton	1.00	0.16	0.18	0.20	0.04	0.19	0.75	0.98	1.18
	Bächlin et al.	1.00	0.15	0.18	0.19	0.04	0.19	0.74	1.04	1.23
Averaged, NO_x background, eq. (17)	Derwent and Middleton	1.00	0.32	0.40	0.40	0.12	0.38	0.74	1.06	2.08
	Bächlin et al.	1.00	0.43	0.56	0.56	0.21	0.55	0.74	1.40	3.35
Averaged, NO_2 background, eq. (18)	Derwent and Middleton	1.00	0.13	0.16	0.20	0.04	0.19	0.74	0.74	0.88
	Bächlin et al.	1.00	0.11	0.14	0.17	0.03	0.16	0.73	0.82	0.91
	Metrics' best value	1	0	0	0	0	0	1	1	0

Identifying the optimal combination of NO_2/NO_x models and calculation decomposition methods is challenging due to the multitude of performance criteria considered. Consequently, a statistical method known as the "critical difference diagram", introduced by Ismail Fawaz et al. (2019), was employed. This method facilitates the comparison of different models by ranking them according to their performance on a given set of criteria (a score of 1 being the best result and 10 the worst). This ranking, which reflects all the performance criteria considered in this work, can then be used to establish critical difference diagrams, as given in Figure 5.

The results indicate that the most effective combinations consistently considered NO_2 background concentrations rather than NO_x, confirming previous findings. Looking specifically at this subgroup, and despite their score being close, the best combinations use averaged predicted concentrations and not hourly ones. Thus, the best calculation decomposition method is the one using both averaged concentrations and NO_2 background concentration (eq. 18). When using this method specifically, the best NO_x/NO_2 model is the Bachlin et al. one, resulting in an overall error to 16 % compared to the measured NO_2 concentrations. Lastly, it appears that the empirical functions considered in this study (Derwent and Middleton and Bachlin et al. models) outperform the photostationary steady-state equilibrium.

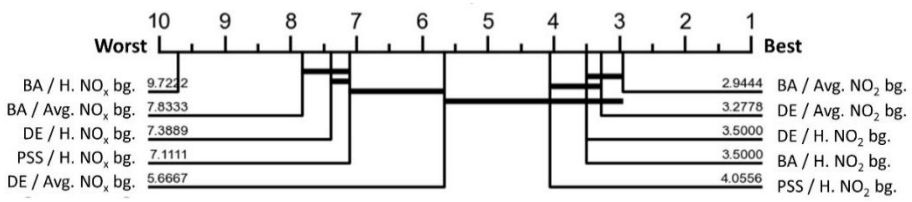

Figure 5. Critical difference diagram of the performance of combinations between NO_2/NO_x model and calculation decomposition considering the whole experimental dataset *(BA: Bachlin et al. model (eq. 14), DE: Derwent and Middleton model (eq. 12-13), PSS: Photostationary Steady State model (eq. 9-11), H. NO_x: Hourly decomposition with NO_x background (eq. 15), H. NO_2: Hourly decomposition with NO_2 background (eq. 16),*

Avg. NO_x: Averaged decomposition with NO_x background (eq. 17) and Avg. NO_2: Averaged decomposition with NO_2 background (eq. 18).

3.2. Quantitative comparison of the NO_2/NO_x models and calculation decompositions results only considering the passive samplers located nearby known traffic emissions.

In this work, microscale modeling is employed through computational fluid dynamics, yielding results that are highly localized and heavily reliant on available information, such as traffic-related emissions. Since traffic emissions are not known for every road segment, and passive sensor results are available where this information is lacking, the predicted NO_2 concentrations were specifically compared with measured NO_2 concentrations from passive sensors located near roads with known traffic emissions. The results of the performance criteria obtained for this specific subset of measured data are given in Table 2.

Based on the outcomes obtained, the same findings as previously noted can be made regarding the ranking capacity of the performance criteria : $FAC2$ and R are not suitable to rank the models or methods; FB, MFB, MFE, $NMSE$ and MRE can be used principally to rank the calculation decomposition methods; and NSE and $Target$ can be used to rank the NO_2/NO_x models.

Improved results were globally obtained across all criteria compared to previous findings. This enhancement can be attributed to the observation that the most significant variations between modeled and measured concentrations occur in areas where emissions are unspecified in the numerical model due to unavailability.

Table 2. Comparison of the NO_x/NO_x models performances as a function of the calculation decomposition considered and only considering the passive samplers located nearby roads where traffic information was available.

Calculation decomposition	**NO_x/NO_2 model**	***FAC2***	***FB***	***MFB***	***MFE***	***NMSE***	***MRE***	***R***	***NSD***	***Target***
Hourly, NO_x background, eq. (15)	PSS	1.00	0.28	0.38	0.38	0.11	0.33	0.78	0.85	1.34
	Derwent and Middleton	1.00	0.43	0.56	0.56	0.21	0.41	0.77	1.59	3.22
	Bächlin et al.	1.00	0.34	0.42	0.42	0.14	0.55	0.77	1.45	2.56
Hourly, NO_2 background, eq. (16)	PSS	1.00	0.05	0.08	0.15	0.02	0.14	0.78	0.80	0.67
	Derwent and Middleton	1.00	0.09	0.11	0.15	0.02	0.14	0.78	1.04	0.84
	Bächlin et al.	1.00	0.09	0.11	0.15	0.02	0.14	0.78	1.11	0.90
Averaged, NO_x background, eq. (17)	Derwent and Middleton	1.00	0.25	0.30	0.30	0.08	0.29	0.77	1.11	1.55
	Bächlin et al.	1.00	0.38	0.48	0.48	0.17	0.46	0.78	1.45	2.69
Averaged, NO_2 background, eq. (18)	Derwent and Middleton	1.00	0.03	0.06	0.15	0.02	0.14	0.78	0.76	0.64
	Bächlin et al.	1.00	0.03	0.05	0.14	0.02	0.13	0.76	0.89	0.68
	Metrics' best value	1	0	0	0	0	0	1	1	0

A critical difference diagram has also been built based on these new results and is given in Figure 6. Again, the best combinations between NO_2/NO_x models and calculation decomposition methods correspond to those where NO_2 background concentrations are used. However, this time, it is no longer obvious whether it is better to consider averaged predicted concentrations rather than hourly ones, or to use empirical methods instead of the PSS. Indeed, while the combination leading to the best results is

still the Bachlin et al. model (eq. 14) associated with averaged predicted concentrations and NO_2 background concentrations (eq. 18), this option is directly followed by the combination of PSS (eq. 9-11) and hourly predicted concentrations (eq. 16). The PSS, inherently more complex than the empirical functions, appears to be more sensitive to the absence of input data, such as traffic emissions.

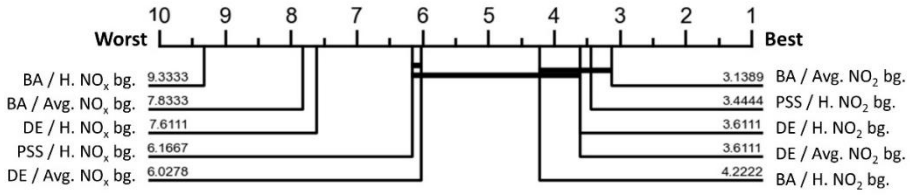

Figure 6. Critical difference diagram of the performance of combinations between NO_2/NO_x model and calculation decomposition considering (A) all samplers and (B) only the samplers located nearby roads where traffic data were available *(BA: Bachlin et al. model (eq. 14), DE: Derwent and Middleton model (eq. 12-13), PSS: Photostationary Steady State model (eq. 9-11), H. NO_x: Hourly decomposition with NO_x background (eq. 15), H. NO_2: Hourly decomposition with NO_2 background (eq. 16), Avg. NO_x: Averaged decomposition with NO_x background (eq. 17) and Avg. NO_2: Averaged decomposition with NO_2 background (eq. 18).*

3.3. Comparison of the monthly NO_2 concentration maps obtained using two extreme combinations of NO_x/NO_2 models and calculation decomposition methods.

Finally, monthly modeled NO_2 concentration maps were generated and compared using two NO_2/NO_x models: the PSS and the Bachlin et al. model, along with various calculation decomposition methods.

According to the results, which can be seen in Figure 7 (A1-B1), NO_2 concentrations are globally underestimated when considering the NO_x background concentration, even in locations where traffic emissions are known. These underestimations are no longer observed when considering background NO_2 concentration, as shown in Figure 7 (A2-B2), except for areas where sensors are located near roads with unknown traffic emissions (sensors mainly located in the bottom left-hand corner or in the center right-hand corner of the study).

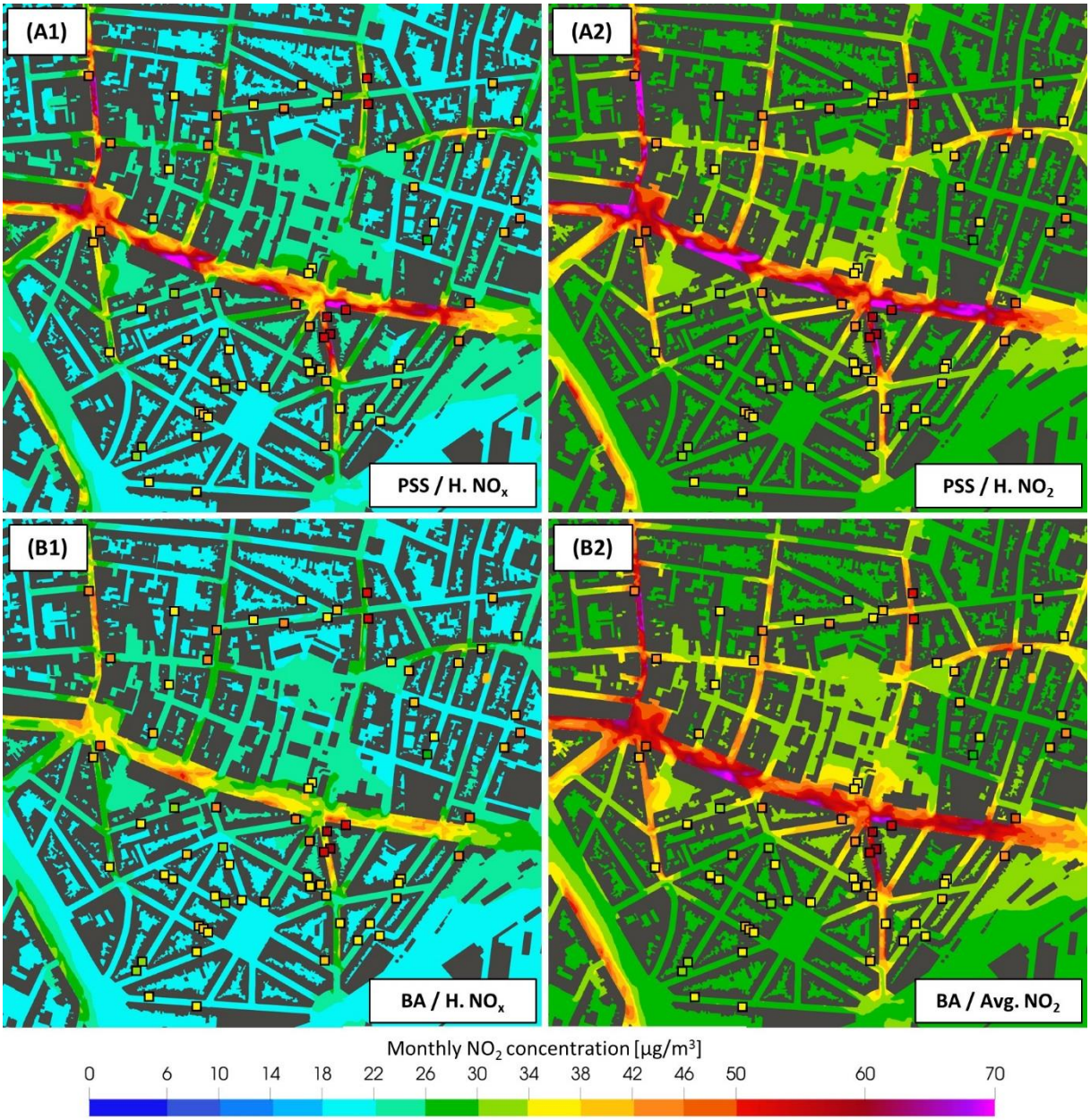

Figure 7. Monthly NO_2 concentration maps obtained by averaging the 696 hourly maps (*BA: Bachlin et al. model (eq. 14), PSS: Photostationary Steady State model (eq. 9-11), H. NO_x: Hourly decomposition with NO_x background (eq. 15), H. NO_2: Hourly decomposition with NO_2 background (eq. 16), and Avg. NO_2: Averaged decomposition with NO_2 background (eq. 18).*

When comparing the results obtained between the two NO_2/NO_x models for the same calculation decomposition method (except for PSS which always need hourly data), such as comparing Figure 7 (A1) with (B1) or Figure 7 (A2) with (B2), it becomes evident that PSS led globally to higher NO_2 concentrations than the Bachlin et al. model. This contrast can be particularly seen in Figure 7 (A1) where NO_2 concentrations exceeding 70 µg/m³ are obtained with the PSS model, while the highest concentrations are around 50 µg/m³ with the Bachlin et al. model as shown in Figure 7 (B1). According to the results shown in Figure 7 (A2), the PSS model tends to overestimate the higher concentrations, with NO_2 concentrations higher than 70 µg/m³ at locations where traffic emissions are known, while sensors show concentrations ranging from 55 to

60 µg/m^3. The Bachlin et al. model achieved closer results than the PSS model, with NO_2 concentrations around 60 µg/m^3 at the exact same location.
Lastly, regardless of the decomposition method or the NO_2/NO_x model considered, underestimations of NO_2 concentrations are systematically observed at some specific locations, for example in the southern part of the area. These locations correspond to sensors positioned near roads where traffic data, and therefore emissions, are not known (see Figure 1 for the detailed locations), thus explaining the underestimation of NO_2 concentrations observed.

4. Discussion

All the simulations were performed considering an isothermal atmosphere (i.e., neutral atmospheric stability), and good results with around 15 % of error overall were obtained when using the right combination of NO_2/NO_x model and calculation decomposition method. This result is interesting because a neutral atmosphere was observed for only 38% of the total duration of the measurement campaign, according to meteorological data. Utilizing an isothermal model is more convenient for various reasons, such as reduced calculation time, improved convergence, and the ability to interpolate results based on wind speed, among others. However, in this case, the three stability states (stable, neutral, and unstable) were roughly equally represented (~33%). In this way, underestimations and overestimations resulting from modeling a neutral case rather than stable and unstable cases could have offset each other. Further work could be conducted, at a different location where stability states are not equally represented, or ideally, at the same location but during months when stable or unstable atmospheres are more predominant.

Additionally, previous results raise questions about the general applicability of the models and methods assessed in this study. Indeed, they have only been tested using one given CFD model and no other CFD models or alternative modeling approaches. However, recent work using artificial intelligence modeling for air quality modeling has shown that the use of empirical methods such as those used in this study, combined with an hourly calculation of NO_2 concentrations and the use of a background NO_2 concentration, led to the same order of magnitude of errors (~ 20 %) (Jurado et al., 2023b). It is therefore reasonable to be expected that these results will be relevant to a wider range of micro-scale models.

It is also important to bear in mind that the deviation between modeled and measured concentrations (< 15%) using the optimum NO_2/NO_x model and the optimum decomposition method is also dependent on the various choices inherent to the numerical model, and particularly the turbulent Schmidt number (set to 0.7) and the turbulence model (RNG k-epsilon) used. One of the aims of this study was to assess the validity of using classical assumption in a real study case. To optimize the model and refine the results, further investigations should be considered by a sensitivity study to determine the best turbulent Schmidt number and turbulence model to use. Therefore, it is important to note that modifications in these parameters would lead to variations in the results, both in terms of increasing the deviation between measured and modelled results or reducing it.

Finally, multiple performance criteria were calculated in this study, including criteria where acceptance thresholds are given for urban dispersion model evaluation and used to validate numerical air quality models on a regular basis. The criteria and corresponding threshold values for urban cases are $|FB| \leq 0.67$, $NMSE \leq 6$ and $FAC2 \geq 0.3$ (Hanna and Chang, 2012). Based on the study's results, all considered NO_2/NO_x models and calculation decomposition methods met the acceptance criteria. This includes combinations of models and methods that resulted in an average error exceeding 50%, surpassing the European Union's minimum accuracy threshold of 30% for annual NO_2 concentration modeling (EU, 2008). Consequently, these initially

established thresholds, meant to validate Lagrangian and Gaussian models, may not be suitable for assessing the quality of micro-scale air quality models, such as computational fluid dynamics or artificial intelligence models. Alternative criteria or acceptance thresholds should be considered instead. For example, the criteria and corresponding acceptance thresholds of $Target \leq 0.65$ (target value) and $Target \leq 0.8$ (critical value) (Thunis et al., 2012) would be better indicators, as being more stringent, since only a few combinations of NO_2/NO_x models and calculation decomposition methods assessed in this work complied with. In any case, these results also underscore the importance of using multiple criteria simultaneously, as relying on a single criterion may lead to potentially misleading conclusion.

5. Conclusion

Simple and fast methods for calculating NO_2 concentrations maps from NO_x computational fluid dynamics results were evaluated through 18 numerical simulations performed under classical CFD air quality modeling assumptions. The main conclusions are as follows.

(a) Fast and simple methods such as photostationary steady-state equilibrium (PSS) or Derwent and Middleton and Bachlin et al. empirical functions can be used to assess NO_2 concentrations from NO_x CFD results. This can be achieved without having to consider complex chemical mechanisms, while satisfying air quality model acceptance criteria.

(b) The best results are achieved using the Bachlin et al. empirical function after averaging the hourly modeled NO_x concentration and adding the NO_2 background concentrations at the final stage, leading to errors of around 16 % and up to 14 % when all traffic emissions are known. One notable advantage is that it only requires NO_x concentration as an input parameter.

(c) PSS gives good results but tends to overestimate NO_2 concentrations while needing numerous additional parameters in addition to the NO_x concentration (O_3 concentration, temperature, etc.).

(d) Classical CFD air quality modeling assumptions such as neutral atmosphere modeling (isothermal conditions), or taking a turbulent Schmidt number of 0.7, led to results that meet air quality model acceptance criteria, with less than 20% error overall when using the correct calculation decomposition method.

References

Agathokleous, E., Sicard, P., 2021. Editorial overview: Current and future challenges of air pollution. Current Opinion in Environmental Science & Health 21, 100246. https://doi.org/10.1016/j.coesh.2021.100246

AIRPARIF, 2016. Inventaire régional des émissions en Île-de-France - Année de référence 2012 - éléments synthétiques - Édition mai 2016 32.

Bächlin, W., Bösinger, R., Brandt, A., Schultz, T., 2008. Überprüfung des NO-NO2-Umwandlungsmodells für die Anwendung bei Immissionsprognosen für bodennahe Stickoxidfreisetzung. Reinhaltung der Luft 66, 154–157.

Blocken, B., 2014. 50 years of Computational Wind Engineering: Past, present and future. Journal of Wind Engineering and Industrial Aerodynamics 129, 69–102. https://doi.org/10.1016/j.jweia.2014.03.008

Chen, H., Kwong, J.C., Copes, R., Tu, K., Villeneuve, P.J., van Donkelaar, A., Hystad, P., Martin, R.V., Murray, B.J., Jessiman, B., Wilton, A.S., Kopp, A., Burnett, R.T., 2017. Living near major roads and the incidence of dementia, Parkinson's disease, and multiple sclerosis: a population-based cohort study. The Lancet 389, 718–726. https://doi.org/10.1016/S0140-6736(16)32399-6

De Craemer, S., Vercauteren, J., Fierens, F., Lefebvre, W., Meysman, F.J.R., 2020. Using Large-Scale NO2 Data from Citizen Science for Air-Quality Compliance and Policy Support. Environ. Sci. Technol. 54, 11070–11078. https://doi.org/10.1021/acs.est.0c02436

Derwent, R.G., Middleton, D.R., 1996. An empirical function for the ratio [NO2]:[NOx]. Clean Air 26, 57–60.

Dickerson, R.R., Stedman, D.H., Delany, A.C., 1982. Direct measurements of ozone and nitrogen dioxide photolysis rates in the troposphere. Journal of Geophysical Research 87, 4933. https://doi.org/10.1029/JC087iC07p04933

EU, 2008. Directive 2008/50/EC of the european parliament and of the council of 21 May 2008 on ambient air quality and cleaner air for Europe, European Union.

Finkelstein, M.M., Jerrett, M., Sears, M.R., 2004. Traffic Air Pollution and Mortality Rate Advancement Periods. American Journal of Epidemiology 160, 173–177. https://doi.org/10.1093/aje/kwh181

Franke, J., Hellsten, A., Schlünzen, H., Carissimo, B., 2007. Best practice guideline for the CFD simulation of flows in the urban environment. COST Action 732.

Hahmann, A., Lennard, C., Badger, J., Vincent, C., Kelly, M., Volker, P., Agent, B., Refslund, J., 2015. Mesoscale modeling for the Wind Atlas of South Africa (WASA) project. https://doi.org/10.13140/RG.2.1.3735.6887

Hanna, S., Chang, J., 2012. Acceptance criteria for urban dispersion model evaluation. Meteorol Atmos Phys 116, 133–146. https://doi.org/10.1007/s00703-011-0177-1

Hanrahan, P.L., 1999. The Plume Volume Molar Ratio Method for Determining NO2/NOx Ratios in Modeling—Part I: Methodology. Journal of the Air & Waste Management Association 49, 1324–1331. https://doi.org/10.1080/10473289.1999.10463960

Ismail Fawaz, H., Forestier, G., Weber, J., Idoumghar, L., Muller, P.-A., 2019. Deep learning for time series classification: a review. Data Min Knowl Disc 33, 917–963. https://doi.org/10.1007/s10618-019-00619-1

Janssen, S., Dumont, G., Fierens, F., Mensink, C., 2008. Spatial interpolation of air pollution measurements using CORINE land cover data. Atmospheric Environment 42, 4884–4903. https://doi.org/10.1016/j.atmosenv.2008.02.043

Jurado, X., Reiminger, N., Maurer, L., José, V., Wemmert, C., 2023a. On the Correlations between Particulate Matter: Comparison between Annual/Monthly Concentrations and PM10/PM2.5. Atmosphere 14, 385.

Jurado, X., Reiminger, N., Maurer, L., Vazquez, J., Wemmert, C., 2023b. Assessment of a deep learning model for monitoring atmospheric pollution: Case study in

Antwerp, Belgium. Sustainable Cities and Society 99, 104951. https://doi.org/10.1016/j.scs.2023.104951

Jurado, X., Reiminger, N., Vazquez, J., Wemmert, C., Dufresne, M., Blond, N., Wertel, J., 2020. Assessment of mean annual NO2 concentration based on a partial dataset. Atmospheric Environment 221, 117087. https://doi.org/10.1016/j.atmosenv.2019.117087

Kluková, Z., Nosek, Š., Fuka, V., Jaňour, Z., Chaloupecká, H., Ďoubalová, J., 2021. The combining effect of the roof shape, roof-height non-uniformity and source position on the pollutant transport between a street canyon and 3D urban array. Journal of Wind Engineering and Industrial Aerodynamics 208, 104468. https://doi.org/10.1016/j.jweia.2020.104468

Koutsourakis, N., Bartzis, J.G., Markatos, N.C., 2012. Evaluation of Reynolds stress, k-ε and RNG k-ε turbulence models in street canyon flows using various experimental datasets. Environmental Fluid Mechanics 12, 379–403. https://doi.org/10.1007/s10652-012-9240-9

Leighton, P.A., 1961. Photochemistry of air pollution, Physical chemistry. New-York Acad.

Li, Z., Zhang, H., Wen, C.-Y., Yang, A.-S., Juan, Y.-H., 2020. Effects of height-asymmetric street canyon configurations on outdoor air temperature and air quality. Building and Environment 183, 107195. https://doi.org/10.1016/j.buildenv.2020.107195

Manisalidis, I., Stavropoulou, E., Stavropoulos, A., Bezirtzoglou, E., 2020. Environmental and Health Impacts of Air Pollution: A Review. Frontiers in Public Health 8.

Pantusheva, M., Mitkov, R., Hristov, P.O., Petrova-Antonova, D., 2022. Air Pollution Dispersion Modelling in Urban Environment Using CFD: A Systematic Review. Atmosphere 13, 1640. https://doi.org/10.3390/atmos13101640

Papageorgakis, G.C., Assanis, D.N., 1999. COMPARISON OF LINEAR AND NONLINEAR RNG-BASED k-epsilon MODELS FOR INCOMPRESSIBLE TURBULENT FLOWS. Numerical Heat Transfer, Part B: Fundamentals 35, 1–22. https://doi.org/10.1080/104077999275983

Reiminger, N., Jurado, X., Maurer, L., Vazquez, J., Wemmert, C., 2023. Influence of depressed road configuration on downwind pollutant concentrations: A CFD study under various thermal stability conditions. Journal of Wind Engineering and Industrial Aerodynamics 235, 105361. https://doi.org/10.1016/j.jweia.2023.105361

Reiminger, N., Jurado, X., Vazquez, J., Wemmert, C., Blond, N., Dufresne, M., Wertel, J., 2020a. Effects of wind speed and atmospheric stability on the air pollution reduction rate induced by noise barriers. Journal of Wind Engineering and Industrial Aerodynamics 200, 104160. https://doi.org/10.1016/j.jweia.2020.104160

Reiminger, N., Jurado, X., Vazquez, J., Wemmert, C., Blond, N., Wertel, J., Dufresne, M., 2020b. Methodologies to assess mean annual air pollution concentration combining numerical results and wind roses. Sustainable Cities and Society 59, 102221. https://doi.org/10.1016/j.scs.2020.102221

Reiminger, N., Vazquez, J., Blond, N., Dufresne, M., Wertel, J., 2020c. CFD evaluation of mean pollutant concentration variations in step-down street canyons. Journal of Wind Engineering and Industrial Aerodynamics 196, 104032. https://doi.org/10.1016/j.jweia.2019.104032

Richards, P.J., Hoxey, R.P., 1993. Appropriate boundary conditions for computational wind engineering models using the k-E turbulence model 9.

Richards, P.J., Norris, S.E., 2011. Appropriate boundary conditions for computational wind engineering models revisited. Journal of Wind Engineering and Industrial Aerodynamics 99, 257–266. https://doi.org/10.1016/j.jweia.2010.12.008

Rivas, E., Santiago, J.L., Lechón, Y., Martín, F., Ariño, A., Pons, J.J., Santamaría, J.M., 2019. CFD modelling of air quality in Pamplona City (Spain): Assessment, stations spatial representativeness and health impacts valuation. Science of the Total Environment 19.

Sanchez, B., Santiago, J.L., Martilli, A., Martin, F., Borge, R., Quaassdorff, C., de la Paz, D., 2017. Modelling NOX concentrations through CFD-RANS in an urban hot-spot using high resolution traffic emissions and meteorology from a mesoscale model. Atmospheric Environment 163, 155–165. https://doi.org/10.1016/j.atmosenv.2017.05.022

Sanchez, B., Santiago, J.-L., Martilli, A., Palacios, M., Kirchner, F., 2016. CFD modeling of reactive pollutant dispersion in simplified urban configurations with different chemical mechanisms. Atmos. Chem. Phys. 16, 12143–12157. https://doi.org/10.5194/acp-16-12143-2016

Santiago, J.L., Martilli, A., Martin, F., 2017. On Dry Deposition Modelling of Atmospheric Pollutants on Vegetation at the Microscale: Application to the Impact of Street Vegetation on Air Quality. Boundary-Layer Meteorology 162, 451–474. https://doi.org/10.1007/s10546-016-0210-5

Schatzmann, M., Leitl, B., 2011. Issues with validation of urban flow and dispersion CFD models. Journal of Wind Engineering and Industrial Aerodynamics 99, 169–186. https://doi.org/10.1016/j.jweia.2011.01.005

Sudalma, S., Purwanto, P., Santoso, L.W., 2015. The Effect of SO2 and NO2 from Transportation and Stationary Emissions Sources to SO42− and NO3− in Rain Water in Semarang. Procedia Environmental Sciences, Basic Researches in The Tropical and Coastal Region Eco Developments 23, 247–252. https://doi.org/10.1016/j.proenv.2015.01.037

Thunis, P., 2018. On the validity of the incremental approach to estimate the impact of cities on air quality. Atmospheric Environment 173, 210–222. https://doi.org/10.1016/j.atmosenv.2017.11.012

Thunis, P., Georgieva, E., Pederzoli, A., 2012. A tool to evaluate air quality model performances in regulatory applications. Environmental Modelling & Software 38, 220–230. https://doi.org/10.1016/j.envsoft.2012.06.005

Tominaga, Y., Stathopoulos, T., 2017. Steady and unsteady RANS simulations of pollutant dispersion around isolated cubical buildings: Effect of large-scale fluctuations on the concentration field. Journal of Wind Engineering and Industrial Aerodynamics 165, 23–33. https://doi.org/10.1016/j.jweia.2017.02.001

Tominaga, Y., Stathopoulos, T., 2007. Turbulent Schmidt numbers for CFD analysis with various types of flowfield. Atmospheric Environment 41, 8091–8099. https://doi.org/10.1016/j.atmosenv.2007.06.054

Troen, I., Petersen, E.L., 1989. European wind atlas. Published for the Commission of the European Communities, Directorate-General for Science, Research, and Development, Brussels, Belgium by Risø National Laboratory, Roskilde, Denmark.

United Nations, 2019. World Urbanization Prospects: The 2018 Revision (ST/ESA/SER.A/420). New York: United Nations.

van Zoest, V., Hoek, G., Osei, F., Stein, A., 2020. Bayesian analysis of the short-term association of NO2 exposure with local burden of asthmatic symptoms in children. Science of The Total Environment 720, 137544. https://doi.org/10.1016/j.scitotenv.2020.137544

Vranckx, S., Vos, P., Maiheu, B., Janssen, S., 2015. Impact of trees on pollutant dispersion in street canyons: A numerical study of the annual average effects in Antwerp, Belgium. Science of The Total Environment 532, 474–483. https://doi.org/10.1016/j.scitotenv.2015.06.032

WHO, 2021. WHO global air quality guidelines: particulate matter (PM2.5 and PM10), ozone, nitrogen dioxide, sulfur dioxide and carbon monoxide. World Health Organization.

WHO (Ed.), 2005. WHO Air quality guidelines for particulate matter, ozone, nitrogen dioxide and sulfur dioxide. Global update 2005. World Health Organization.

Wu, J., Ye, Q., Fang, L., Deng, L., Liao, T., Liu, B., Lv, X., Zhang, J., Tao, J., Ye, D., 2022. Short-term association of NO2 with hospital visits for chronic kidney disease and effect modification by temperature in Hefei, China: A time series study. Ecotoxicology and Environmental Safety 237, 113505. https://doi.org/10.1016/j.ecoenv.2022.113505

Xiaomin, X., Huang, Z., Wang, J., 2006. The impact of urban street layout on local atmospheric environment. Building and Environment 41, 1352–1363. https://doi.org/10.1016/j.buildenv.2005.05.028

Yakhot, V., Orszag, S.A., Thangam, S., Gatski, T.B., Speziale, C.G., 1992. Development of turbulence models for shear flows by a double expansion technique. Physics of Fluids A: Fluid Dynamics 4, 1510–1520. https://doi.org/10.1063/1.858424

Yang, J., Shi, B., Shi, Y., Marvin, S., Zheng, Y., Xia, G., 2020. Air pollution dispersal in high density urban areas: Research on the triadic relation of wind, air pollution, and urban form. Sustainable Cities and Society 54, 101941. https://doi.org/10.1016/j.scs.2019.101941

Yuan, Y., Yang, K., Du, C., Fu, X., 2017. Study on Schmidt Number of Pollutant Diffusion in Urban Street Atmosphere. Procedia Engineering 205, 1711–1717. https://doi.org/10.1016/j.proeng.2017.10.368

Yue, H., Yang, X., Ji, X., Wu, X., Li, G., Sang, N., 2022. Time series of transcriptome analysis in entire lung development stages provide insights into the origin of NO2 related lung diseases. Environment International 168, 107454. https://doi.org/10.1016/j.envint.2022.107454